DESIGN OF A LAMBDA CONFIGURATION IN ARTIFICIAL COHERENT NANOSTRUCTURES*

P.G. DI STEFANO[1], E. PALADINO[1,2,3], A. D'ARRIGO[1,2], B. SPAGNOLO[4,3], G. FALCI[1,2,3]

[1]Dipartimento di Fisica e Astronomia, Università di Catania, Via Santa Sofia 64, 95123 Catania, Italy
[2]CNR-IMM UOS Università (MATIS), Consiglio Nazionale delle Ricerche,
Via Santa Sofia 64, 95123 Catania, Italy
[3]Istituto Nazionale di Fisica Nucleare, Via Santa Sofia 64, 95123 Catania, Italy
[4]Dipartimento di Fisica e Chimica, Università di Palermo, Group of Interdisciplinary Physics and
CNISM, Unità di Palermo, Viale delle Scienze, Ed.18, I-90128 Palermo, Italy

Received March 8, 2015

The implementation of a three-level Lambda System in artificial atoms would allow to perform advanced control tasks typical of quantum optics in the solid state realm, with photons in the μm/mm range. However hardware constraints put an obstacle since protection from decoherence is often conflicting with efficient coupling to external fields. We address the problem of performing conventional STImulated Raman Adiabatic Passage (STIRAP) in the presence of low-frequency noise. We propose two strategies to defeat decoherence, based on "optimal symmetry breaking" and dynamical decoupling. We suggest how to apply to the different implementations of superconducting artificial atoms, stressing the key role of non-Markovianity.

1. INTRODUCTION

In recent years several experiments have demonstrated multilevel coherence in superconducting artificial atoms, as the observation of the Autler-Townes (AT) [1, 2] effect, of electromagnetically induced transparency (EIT) [3], besides evidences of three-state superpositions [4] and coherent population trapping (CPT) [5]. Further exploiting coherence in such systems would be important in principle and moreover allow important applications in solid-state quantum integrated coherent architectures. So far all the experiments in these systems (except the one of Ref. [5]) have been performed driving by ac-fields in *ladder* configuration (see Fig. 1a). In this work we address the design of a *lambda* configuration in three-level artificial atoms which would allow to implement tasks [6–8] where two-photon absorption *and* emission are involved at once. Despite of several theoretical proposal [9–13], this goal is still experimentally unsettled, mainly because protection from low-frequency noise requires to enforce exact or approximate symmetries of the Hamiltonian, which on the other hand imply selection rules canceling the pump coupling [8, 9, 12] (see Fig. 1a).

*Paper presented at the conference "Advanced many-body and statistical methods in mesoscopic systems II", September 1-5, 2014, Brasov, Romania.

Rom. Journ. Phys., Vol. 60, Nos. 5-6, P. 676–685, Bucharest, 2015

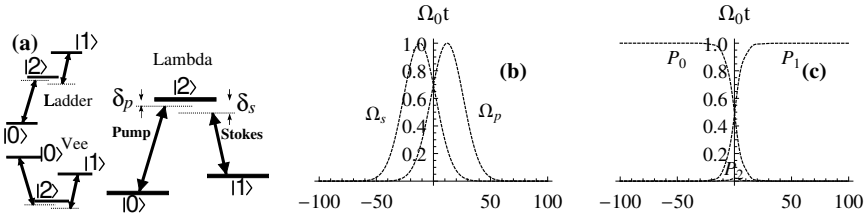

Fig. 1 – (a) Three-level system driven with AC fields in Λ configuration (in the insets the Ladder and the Vee configurations). (b) Gaussian pulses in the counterintuitive sequence (here $\Omega_0 T = 20, \tau = 0.6T$). (c) Population histories $P_i(t) = |\langle i|\psi(t)\rangle|^2$ for ideal STIRAP ($\delta = 0$) and for $\delta_p = -0.2\,\Omega_0$, $\kappa = 1$.

Our second goal of is to elucidate the central role of non-Markovian noise in producing three-level decoherence for the class of phenomena based on CPT. We focus on a protocol called STIRAP [14, 15], described in Sec.2, which involves several basic coherent effects and allows striking applications in integrated atom-cavity systems. Therefore its demonstration would be a benchmark for multilevel advanced control in artificial atoms. In Sec. 3 we introduce an effective model for noise and argue that dephasing in the "trapped subspace" $\mathrm{span}\{|0\rangle, |1\rangle\}$ (see Fig. 1a) plays the major role. We show that implementation of STIRAP in Lambda configuration is possible within present technology. In Sec. 4 we propose two strategies to defeat dephasing, namely the search for optimal symmetry breaking conditions, and selective dynamical decoupling of noise sources achieved by operating on a specific external control. Both strategies leverage on the fact that dephasing in the solid state is due to broad band colored noise (BBCN), which is inherently non-Markovian. As a consequence BBCN impacts on dephasing in a way specific of correlations of the induced fluctuations of the device bandstructure. Finally, in Sec.6 we conclude and discuss some further perspective.

2. COHERENT POPULATION TRANSFER IN THREE-LEVEL ATOMS

STIRAP is an advanced control technique of $M > 2$-level systems, allowing complete population transfer between two states $|0\rangle$ and $|1\rangle$, even in absence of a direct coupling, *via* one or more intermediate states which are *never* populated. In three-level systems the indirect linkage is provided by the typical configurations of two ac-fields shown in Fig. 1a. The pump field at $\omega_p \approx |E_2 - E_0|$, triggers transitions $|0\rangle \leftrightarrow |2\rangle$ whereas the Stokes, $\omega_s \approx |E_2 - E_1|$, triggers $|1\rangle \leftrightarrow |2\rangle$ ones. The standard Hamiltonian in the rotating wave approximation (RWA) in a rotating frame referred to the "bare" basis $\{|0\rangle, |1\rangle, |2\rangle\}$ is given by the matrix

$$H = \begin{bmatrix} 0 & 0 & \frac{1}{2}\Omega_p^*(t) \\ 0 & \delta(t) & \frac{1}{2}\Omega_s^*(t) \\ \frac{1}{2}\Omega_p(t) & \frac{1}{2}\Omega_s(t) & \delta_p(t) \end{bmatrix}, \tag{1}$$

where the Rabi frequencies $\Omega_k(t)$ for $k = p, s$ are related to the amplitudes of the pump and Stokes fields, δ_k are the single-photon detunings and $\delta = \delta_p - \delta_s$ is the two-photon detuning. We will mostly refer to the Lambda configurations where $\delta_p(t) := E_2 - E_0 - \omega_p$ and $\delta_s(t) := E_2 - E_1 - \omega_s$. At two-photon resonance, $\delta = 0$, the Hamiltonian (1) has an instantaneous eigenvector with null eigenvalue, $\epsilon_0 = 0$, given by $|D\rangle = (\Omega_s |0\rangle - \Omega_p |1\rangle)/\sqrt{\Omega_s^2 + \Omega_p^2}$. It is called the "dark state" since state $|2\rangle$ is not populated, despite of the transitions triggered by the fields. In ideal STIRAP ($\delta = 0$) adiabatic pulses $\Omega_k(t)$ are shined in the *counterintuitive* sequence, *i.e.* the Stokes preceding the pump. We will make use of Gaussian pulses

$$\Omega_p = \kappa_p \Omega_0 \, \mathrm{e}^{-[(t+\tau)/T]^2} \qquad \Omega_s = \kappa_s \Omega_0 \, \mathrm{e}^{-[(t-\tau/T]^2} \tag{2}$$

with $\tau \sim T$. Here Ω_0 is a frequency scale and $\kappa_k \sim 1$ are constants which will be taken equal to 1 when not otherwise specified. In this way the dark state $|D(t)\rangle$ (Fig. 1b) performs the desired $|0\rangle \to |1\rangle$ evolution, yielding complete population transfer, while $|2\rangle$ is never populated (Fig. 1d). Adiabaticity in ideal STIRAP [14,

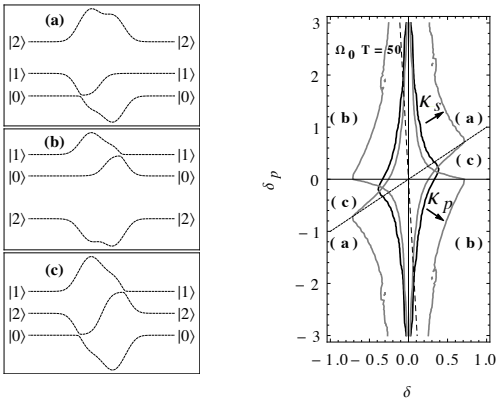

Fig. 2 – Left panel: typical Landau-Zener (LZ) patterns as a function of time of instantaneous eigenvalues for nonzero detunings. Three different patterns may occur according to the value of δ_p/δ (see Sec.4). Right panel: efficiency diagram of STIRAP *vs.* detunings. The curves enclose regions corresponding to efficiency larger than 90%. The black line is obtained for $\kappa_p = \kappa_s$ and shows that the protocol is much more sensitive to deviations of δ rather than of δ_p. Gray lines are the efficiencies when $\kappa_p = 2\kappa_s$ and $\kappa_s = 2\kappa_p$ (see Sec. 4). Intercepts of such curves with lines $\delta_p/\delta = a$ define the two-photon linewidths $\delta_{\frac{1}{2}}$ as a function of all the parameters but δ. The dashed line shows the example of the Cooper pair box for $q_g = 0.48$ and $J = 1$.

15] requires that $\Omega_0 T > 10$. Since it involves in a clever sequence several coherent phenomena [15] (AT effect, EIT and adiabatic passage), STIRAP is very efficient, faithful and stable apart for a crucial sensitivity to δ (see Fig. 2 right panel). Indeed for $\delta \neq 0$ no exact dark state exists providing the adiabatic connection $|0\rangle \to |1\rangle$. Still population transfer may take place by *non-ideal STIRAP*, *via* non-adiabatic Landau-

Zener (LZ) transitions between adiabatic states (see Fig. 2 left panel), a mechanism crucial for the applications in artificial atoms (Sec.4).

In artificial atoms the Hamiltonian reads [11, 16] $H = H_0(\mathbf{q}) + [\mathcal{A}_p(t)\cos(\omega_p t) + \mathcal{A}_s(t)\cos(\omega_s t)]\mathcal{P}$, where the device H_0 depends on tunable parameters $\mathbf{q}$. The field couples to the system operator $\mathcal{P}$ and the envelopes $\mathcal{A}_k(t), k = p, s$ are slowly varying with respect to Rabi frequencies. Under suitable conditions, H can be truncated to three levels. Performing the RWA and transforming to a doubly rotating frame, we get the form (1), where $\Omega_p(t) = \mathcal{A}_p(t)\,\mathcal{P}_{20}$ and $\Omega_s(t) = \mathcal{A}_s(t)\,\mathcal{P}_{21}$.

3. EFFECTIVE MODEL FOR SOLID-STATE NOISE

Physically, noise in solid-state devices has large low-frequency components with a $1/f^\alpha$ spectrum, and high frequency component, either white or ohmic. Assuming for simplicity a single noise source inducing fluctuations of the parameter q_g, we can describe this BBCN by the phenomenological Hamiltonian [16] $H = H_0(q_g + x(t)) + \mathcal{A}(t)\mathcal{P} + H_{env}$. Here $x(t)$ is a classical stochastic process accounting for low-frequency noise, whereas H_{env} describes an environment coupled to the system, responsible for Markovian quantum noise. The effect of low-frequency noise is obtained by averaging over the stochastic process the density matrix $\rho^f(t|q_g + x(t))$, accounting for fast noise in a background stochastic field

$$\rho(t) = \int \mathcal{D}x(t)\, P[x(t)]\; \rho^f(t|q_g + x(t)) \tag{3}$$

Leading effects are estimated by evaluating the integral in the "quasistatic" or static path approximation (SPA), *i.e.* by substituting $x(t)$ with a random variable x with distribution $p(x)$ and calculating $\rho^f(t|q_g + x)$ by a Markovian master equation.

Notice that H_0, its eigen-energies $E_i(q_g)$ and the matrix elements P_{ij} entering $\Omega_{ij}(q_g)$ depend on q_g. A proper choice of q_g may enforce symmetries of H, which protect the system against dephasing due to fluctuations of $E_i(q_g)$, but at the same time suppress some P_{ij}. Non-Markovian noise determines fluctuations of the entries of the Hamiltonian (1), namely $\delta_k(q_g + x) = \Delta E_k(q_g + x) - \omega_k$ and $\Omega_k(q_g + x) = \mathcal{A}_k(t)\,\mathcal{P}_k(q_g + x)$, where $\Delta E_k(q_g + x)$ and $\mathcal{P}_k(q_g + x)$ are the relevant energy splittings and "dipole" matrix elements. This is a key issue for all our subsequent analysis about design and optimization of Lambda systems. For instance, it is clear that for a Lambda configuration at nominal resonance, *i.e.* if external fields are resonant at the nominal bias q_g, fluctuations in the "trapped subspace" translate in stray $\delta \neq 0$ which are the most detrimental for STIRAP. It is convenient to expand detunings and Rabi frequencies. For instance at nominal resonance and for small enough fluctuations, imposing $E_0 = 0$ we have

$$\delta(x) = A_1(\mathbf{q})x + \frac{1}{2}B_1(\mathbf{q})x^2 \quad ; \quad \delta_p(x) = \Delta E_2 = A_2(\mathbf{q})x + \frac{1}{2}B_2(\mathbf{q})x^2 \tag{4}$$

where $A_i(\mathbf{q}) = \partial E_i(\mathbf{q})/\partial q_g$ and $B_i(\mathbf{q}) = \partial^2 E_i(\mathbf{q})/\partial q_g^2$. We notice that all such fluctuations are correlated *via* the bandstructure of the device, since they originate from the same random variable x.

We apply these ideas to the important case study of the Cooper pair box (CPB), a superconducting device described by the Hamiltonian

$$H_0(q_g, J) = \sum_n (q_g - n)^2 |\phi_n\rangle\langle\phi_n| - \frac{J}{2}(|\phi_{n+1}\rangle\langle\phi_n| + h.c.). \tag{5}$$

Here $\hat{n} := \sum_n n\,|\phi_n\rangle\,\langle\phi_n|$ is the number of extra Cooper pairs in a metallic island. The parameter J is the relative strength of the Josepson tunneling changing $n \to n \pm 1$. According to its value several different implementations of superconducting qubits from "charge qubits" to "transmons" [17–21] have been demonstrated. The other parameter q_g can be tuned by an external voltage. The CPB is operated by an ac gate voltage which is coupled to the charge, $\mathcal{P} = 2e\hat{n}$, playing the role of the system operator.

The Hamiltonian $H_0(q_g, J) = \sum_i E_i\,|i\rangle\,\langle i|$ is symmetric for charge parity transformations at half-integer and integer q_g. Here the selection rule $n_{ij} := \langle i|\,\hat{n}\,|j\rangle = [1 - (-1)^{i+j}]n_{ij}$ holds, preventing pump coupling. On the other hand working at $q_g = 1/2$ guarantees the maximal protection from charge noise because of the suppression of $A_i(\mathbf{q})$ in Eq.(4). Larger values of $J \gg 1$ suppress asymmetries at $q_g \neq 1/2$, ensuring protection in a larger region of the space of parameters, where however the pump coupling is suppressed [12].

The numerically calculated [12] efficiency of STIRAP (Fig. 3a) shows that a Lambda configuration allowing population transfer $\sim 80\%$ is achievable in a CPB with $J = 1$ by operating at a symmetry breaking bias $q_g \neq 1/2$, despite of the reduced protection from low-frequency noise. In this regime, $q_g \lesssim 0.49$, only linear fluctuation of detunings matter, *i.e.* linear terms in Eqs.(4) are considered. We used $\Omega_0 T = 15$ to guarantee good adiabaticity, with figures of noise and couplings consistent with measurements of the decoherence in the qubit of Ref. [22]. In this regime, Markovian emission [14, 15] or absorption [12] channels are not effective, whereas spontaneous decay in the trapped subspace, characterized by T_1, is tolerably small. Instead near $q_g = 1/2$ pump coupling is small and it would require $T \gg T_1$, thereby decay suppresses the efficiency.

4. STRATEGIES OF PROTECTION AGAINST NOISE

We now analyze the trade-off between efficient coupling and decoherence when parity symmetry is broken. Our analysis leverages on the results of last section, that the main mechanism of efficiency loss (besides lack of adiabaticity) are low-frequency fluctuations of energy levels. As discussed in Sec.3, these correspond to

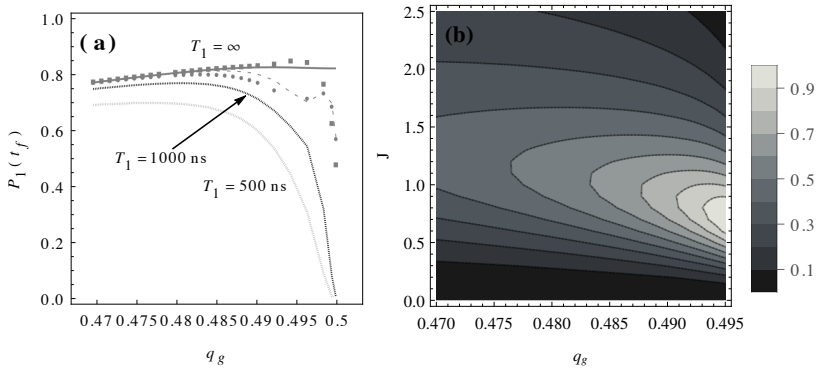

Fig. 3 – (a) Efficiency of STIRAP in the CPB for $J = 1$, showing the effect of low-frequency noise alone and with additional Markovian noise. Field amplitudes, corresponding to Rabi oscillations $\Omega_R = 2\pi \cdot 600\mathrm{rad/s}$ in the Quantronium qubit [22] operated at the symmetry point, yield a sufficiently large pump frequency $\Omega_0 \simeq \Omega_R n_{02}(q_g)/n_{01}(0.5)$ for values of q_g which slightly break the symmetry. Here we consider linear fluctuations of detunings (thick solid line), while adding their quadratic fluctuations (squares) and fluctuations of Ω_k in linear (dashed line) and quadratic approximation (dots) has no effect. Markovian noise determines a smaller further reduction of the efficiency (thin gray lines). We used a variance $\sigma_x = 0.004$ of $p(x)$ and $T_1 = 500, 1000\,\mathrm{ns}$ (b) Figure of merit Eq.(6) for design and optimal symmetry breaking against low-frequency charge noise in the CPB. We consider the region where charge noise is linear since closer to the symmetry point $q_g = 1/2$, STIRAP is suppressed by spontaneous decay.

fluctuations of detunings and can be represented on the diagram of Fig. 2 by a curve. For vanishing nominal detunings it has parametric equations (4) and passes the origin for $x = 0$. Notice that in general in artificial atoms fluctuations of detunings produced by a specific noise source show specific correlations. In the linear noise regime $\delta_p/\delta = a$, where $a = A_2(\mathbf{q})/A_1(\mathbf{q})$, thereby the signs of the derivatives $A_i(\mathbf{q})$ of the bandstructure determine whether detunings are correlated (*e.g.* critical current noise in flux qubits) or anti-correlated (*e.g.* charge noise in the CPB) [16]. It has been shown [11] that according to such correlations, three different kind of LZ patterns may occur. They are shown in Fig. 2 (left panel) and labeled with (a) for $\delta_p/\delta > 1$, (b) for $\delta_p/\delta < 0$ and (c) for $0 \leq \delta_p/\delta < 1$. The efficiency dependence on parameters turns out to be different in the three cases, this being the key to classify effects of low-frequency noise and the specific strategies to suppress them.

Since *both* couplings and fluctuations depend on the solution of the eigenproblem of $H_0(\mathbf{q})$, we may seek for an "optimal" set of values $\mathbf{q}$ such that the symmetry breaking yields enough pump coupling still keeping decoherence tolerable. Referring to Fig. 2 we formulate this condition by defining a *two-photon line width* [23] $\delta_{\frac{1}{2}}$, as the interval of δ where coherent transfer is appreciable, for any fixed combination of the other parameters (see Fig. 2). For efficient STIRAP low-frequency noise must

induce fluctuations of δ with small enough variance, $\sigma_\delta \approx \sqrt{A_1^2\sigma_x^2 + \frac{1}{2}B_1^2\sigma_x^4} \lesssim \delta_{1/2}$.

The line width can be estimated by evaluating the impact of unwanted transitions between adiabatic states. In this way Vitanov *et al.* [23] found the scaling law $\delta_{\frac{1}{2}} \simeq d(\tau)\Omega_0\sqrt{\kappa_p^2+\kappa_s^2}$ valid for $\delta_p = 0$, and roughly holding on the lines $\delta_p/\delta = a$ in the region (c) of Fig. 2 left. In the same way one can derive that $\delta_{\frac{1}{2}} \approx d'(\tau,\kappa)\Omega_0\kappa_p$ in the region (b) of anti-correlated detunings [12], whereas $\delta_{\frac{1}{2}} \approx d''(\tau,\kappa)\Omega_0\kappa_s$ in the region (a) of correlated detunings. The dependence on $\kappa = \kappa_s/\kappa_p$ in the prefactors turns out to be weak.

In the case of CPB, since A_1 and A_2 have different sign, charge noise determines anti-correlated fluctuations of detunings, and good transfer efficiencies are achieved for large values of the ratio

$$\frac{\delta_{\frac{1}{2}}}{\sigma_\delta} \propto \frac{\kappa_p\Omega_0}{\sigma_\delta} \approx \frac{2\,n_{02}(J,q_g)}{\sqrt{A_1^2(J,q_g)\sigma_x^2 + \frac{1}{2}B_1^2(J,q_g)\sigma_x^4}}. \tag{6}$$

This is a figure of merit for STIRAP efficiency (see Fig. 3b) which can be used for seeking optimization of both the design of the device and the symmetry breaking of the Hamiltonian modulated on-chip by the bias q_g.

The above analysis also suggests that effects of charge noise in a CPB can be minimized by increasing κ_p only. This is a specific way of decoupling dynamically noise sources, responsible for anti-correlated (δ,δ_p) fluctuations. Indeed it is clear from Fig. 2b (the blue curve) that increasing κ_p the efficiency grows in the region (b), suppressing anti-correlated fluctuations of detunings. This happens because non ideal STIRAP occurs *via* LZ tunneling along the pattern (b) in Fig. 2, being suppressed for increasing δ when the avoided crossing builts on, and being restored if the gap shrinks due to a larger Ω_p.

This analysis can be extended to the main different designs of superconducting artificial atoms, and to each specific low-frequency noise source. These latter are classified according to the (δ,δ_p) correlations they determine. For instance flux noise in flux qubits yields anti-correlated (δ,δ_p), as for charge noise in the CPB, and increasing Ω_p yields dynamical decoupling. Instead critical current noise in CPB and flux qubit determine correlated (δ,δ_p) fluctuations, requiring larger Ω_s. In phase qubits both critical current and bias current noise yield correlated (δ,δ_p) fluctuations dynamically suppressed by a large Ω_s.

In real superconducting artificial atoms, where more than one noise source is present, the two strategies can be combined. Protection from noise producing anti-correlated (δ,δ_p) fluctuations can be achieved by the optimal symmetry breaking strategy, since dynamical decoupling is limited by the insufficient coupling Ω_p. Protection from noise producing correlated (δ,δ_p) fluctuations can then be obtained in-

creasing Ω_s, which is not limited by selection rules.

It is easy to extend this analysis to artificial atoms driven in different field configurations. For instance for population transfer in the Ladder scheme (Fig. 1) scheme one associates δ (δ_p) with the second (first) excited state, which allows to identify the relevant correlations between detunings.

5. IMPLICATIONS OF NON-MARKOVIANITY

The picture of the last section relies on the non-Markovianity of BBCN. We remind that low-frequency noise is the main source of dephasing in artificial atoms. BBCN explains distinctive experimental observations in quantum bits [16, 22, 24, 25]. Moreover design of low-decoherence qubits relies on protection from non-Markovian noise. Both optimal tuning [26, 27] and dynamical decoupling [28, 29] have been exploited for entangled states We generalize this ideas to protection of three-level coherence, obtaining a rich scenario.

It is important to point out the different impact on STIRAP of non-Markovian dephasing, as discussed in this work, and Markovian pure dephasing as described by the standard Master Equation approach. This latter problem has been studied in Ref. [30], including only the dephasing rates $\tilde{\gamma}_{ij}$. For large enough $\Omega_0 T$ populations at the end of the protocol were found to be

$$\rho_{11}(\infty) = \frac{1}{3} + \frac{2}{3}\mathrm{e}^{-3\tilde{\gamma_{01}}T^2/8\tau} \quad ; \quad \rho_{00}(\infty) = \rho_{22}(\infty) = \frac{1}{3} - \frac{1}{3}\mathrm{e}^{-3\tilde{\gamma_{01}}T^2/8\tau} \qquad (7)$$

i.e. dephasing determines efficiency losses which do not depend on the peak Rabi frequencies. Therefore Markovian dephasing cannot at all accout for the scenario presented in Sec. 4.

In Fig. 4 we plot the final populations of the bare states comparing Markovian (ρ_{ii}) and non-Markovian (P_i) pure dephasing, in the entire relevant range of Ω_0. Noise produces in both cases the same qubit dephasing time T_2, which is relatively large. For large Ω_0 while for non-Markovian noise P_1 is completely recovered, for Markovian noise it saturates to a smaller value given by Eq.(7). For small Ω_0 the protocol fails in both cases, due to insufficient adiabaticity.

6. CONCLUSIONS

In this work we discussed effects of BBCN noise in three level artificial atoms. In particular we studied the trade-off between protection from low-frequency noise, enforced by symmetries of the Hamiltonian, and the implied selection rules which are the main obstacle to the implementation of a Lambda scheme. Being based on two-photon absorption *and* emission, the Lambda scheme allows performing tasks as

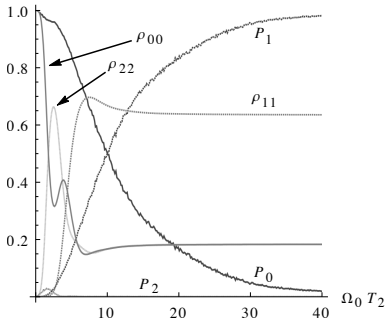

Fig. 4 – Final populations of STIRAP with Markovian (ρ_{ii}) and non Markovian (P_i) noise. The former is the solution of a Master Equation with rate $\tilde{\gamma}_{10} = 1/T_2$, leading to exponential decay of qubit coherences. The non-Markovian noise is simulated taking a distribution of detunings corresponding to $\sigma_x = \sqrt{2}/(A_1 T_2)$, leading to Gaussian decay with the same T_2.

transduction of photons in the μm/mm range. We have studied STIRAP since it is a benchmark advanced protocol. It is also the basis of other protocols from preparation of superpositions [15] to transfer of wave packets and manipulation of photons, with still unexplored potentialities for quantum information and quantum control.

We have shown that model for BBCN noise decoherence in the "trapped subspace" $\mathrm{span}\{|0\rangle, |1\rangle\}$ plays a major role, a conclusion which holds for all Lambda, Ladder and Vee schemes. Strategies to defeat noise in qubits can then be generalized to three-level systems. We presented two strategies, namely optimal symmetry breaking and continuous dynamical decoupling, which can be integrated to minimize the effects of anti-correlated and correlated parametric fluctuations of the artificial atom bandstructure. Relying on non-Markovianity of BBCN, our results suggest that features of the scenario of STIRAP with BBCN, as the predictions on the peculiar dependence on control knobs described in Sec. 4, could be used to probe aspects of non-Markovianity of the solid-state environment.

Finally, we mention that artificial atoms allow for new unconventional schemes to manipulate a Lambda system, bypassing hardware constraints and allowing to perform STIRAP at protected symmetry points and with always-on fields. The strategies to defeat noise presented here could be successfully applied also in these cases.

Acknowledgements. This work was supported by MIUR through Grant. "ENERGETIC – Tecnologie per l'ENERGia e l'Efficienza energETICa", No. PON02_00355_3391233. A.D.A. acknowledges support from Centro Siciliano di Fisica Nucleare e Struttura della Materia under grant MEDNETNA.

REFERENCES

1. M. A. Sillanpää, J. Li, K. Cicak, F. Altomare, J. I. Park, R. W. Simmonds, G. S. Paraoanu, P. J. Hakonen, Phys. Rev. Lett. **103**, 193601 (2009).
2. J. Li, G. Paraoanu, K. Cicak, F. Altomare, J. Park, R. Simmonds, M. Sillanpää, P. Hakonen, Scientific Reports **2**, 645 (2012).
3. A. A. Abdumalikov, O. Astafiev, A. M. Zagoskin, Y. A. Pashkin, Y. Nakamura, J. S. Tsai, Phys. Rev. Lett. **104**, 193601 (2010).
4. R. Bianchetti, S. Filipp, M. Baur, J. M. Fink, C. Lang, L. Steffen, M. Boissonneault, A. Blais, A. Wallraff, Phys. Rev. Lett. **105**, 223601 (2010).
5. W. R. Kelly, Z. Dutton, J. Schlafer, B. Mookerji, T. A. Ohki, J. S. Kline, D. P. Pappas, Phys. Rev. Lett. **104**, 163601 (2010).
6. A. Kuhn, M. Hennrich, T. Bondo, G. Rempe, Appl. Phys. B **69**, 373–377 (1999).
7. M. Mücke, J. Bochmann, C. Hahn, A. Neuzner, C. Nölleke, A. Reiserer, G. Rempe, S. Ritter, Phys. Rev. A **87**, 063805 (2013).
8. J. Siewert, T. Brandes, G. Falci, Optics Communications **264**, 435 – 440 (2006).
9. Y. Liu, J. You, L. Wei, C. Sun, F. Nori, Phys. Rev. Lett. **95** (2005).
10. L. F. Wei, J. R. Johansson, L. X. Cen, S. Ashhab, F. Nori, Phys. Rev. Lett. **100**, 113601 (2008).
11. G. Falci, M. Berritta, A. Russo, A. D'Arrigo, E. Paladino, Phys. Scr. **T151** (2012).
12. G. Falci, A. La Cognata, M. Berritta, A. D'Arrigo, E. Paladino, B. Spagnolo, Phys. Rev. B **87**, 214515–1, 214515–13 (2013).
13. J. Q. You, F. Nori, Nature **474**, 589 (2011).
14. K. Bergmann, H. Theuer, B. Shore, Rev. Mod. Phys. **70**, 1003–1025 (1998).
15. N. V. Vitanov, B. W. S. T. Halfmann, K. Bergmann, Annu. Rev. Phys. Chem. **52**, 763 (2001).
16. E. Paladino, Y. Galperin, G. Falci, B. Altshuler, Rev. Mod. Phys. **86**, 361–418 (2014).
17. Y. Nakamura, Y. A. Pashkin, J. S. Tsai, Nature **398**, 786–788 (1999).
18. T. Duty, D. Gunnarsson, K. Bladh, P. Delsing, Phys. Rev. B **69** (2004).
19. D. Vion, A. Aassime, A. Cottet, P. Joyez, H. Pothier, C. Urbina, D. Esteve, M. H. Devoret, Science **296**, 886–889 (2002).
20. A. Wallraff, D. I. Schuster, A. Blais, L. Frunzio, R. S. Huang, J. Majer, S. Kumar, S. M. Girvin, R. J. Schoelkopf, Nature **421**, 162–167 (2004).
21. J. Koch, T. Yu, J. Gambetta, A. Houck, D. Schuster, J. Majer, A. Blais, M. Devoret, S. Girvin, R. Schoelkopf, Phys. Rev. A **76** (2007).
22. G. Ithier, E. Collin, P. Joyez, P. Meeson, D. Vion, *et al.*, Phys. Rev. B **72** (2005).
23. N. Vitanov, M. Fleischhauer, B. Shore, K. Bergmann, Adv. in At. Mol. and Opt. Phys. **46**, 55–190 (2001).
24. J. Bylander, S. Gustavsson, F. Yan, F. Yoshihara, K. Harrabi, G. Fitch, D. G. Cory, Y. Nakamura, J.-S. Tsai, W. D. Oliver, Nat Phys **7**, 565–570 (2011).
25. F. Charello, E. Paladino, M. G. Castellano, C. Cosmelli, A. D'Arrigo, G. Torrioli, G. Falci, New J. Phys. **14** (2012).
26. E. Paladino, A. D'Arrigo, A. Mastellone, G. Falci, New Jour. Phys. **13** (2011).
27. E. Paladino, A. Mastellone, A. D'Arrigo, G. Falci, Phys. Rev. B **81** (2010).
28. R. Lo Franco, A. D'Arrigo, G. Falci, G. Compagno, E. Paladino, Phys. Scripta **T147** (2012).
29. R. Lo Franco, A. D'Arrigo, G. Falci, G. Compagno, E. Paladino, Phys. Rev. B **90**, 054304 (2014).
30. P. A. Ivanov, N. Vitanov, K. Bergmann, Phys. Rev. A **70**, 063409 (2004).